



Published in final edited form as:

*Knee Surg Sports Traumatol Arthrosc.* 2018 May ; 26(5): 1311–1318. doi:10.1007/s00167-017-4560-4.

## Three-Dimensional Isotropic Magnetic Resonance Imaging Can Provide A Reliable Estimate of The Native Anterior Cruciate Ligament Insertion Site Anatomy

Daisuke Araki<sup>1,2</sup>, Eric Thorhauer<sup>1</sup>, and Scott Tashman<sup>1</sup>

<sup>1</sup>Department of Orthopedic Surgery, University of Pittsburgh, Pittsburgh, PA, USA

<sup>2</sup>Department of Orthopedic Surgery, Kobe University Graduate School of Medicine, Kobe, Japan

### Abstract

**Purpose**—This study quantified the error in anterior cruciate ligament (ACL) insertion site location and area estimated from three-dimensional (3D) isotropic magnetic resonance imaging (MRI) by comparing to native insertion sites determined via 3D laser scanning.

**Methods**—Isotropic 3D DESS MRI was acquired from twelve fresh-frozen, ACL-intact cadaver knees. ACL insertion sites were manually outlined in each MRI slice, and the resulting contours combined to determine the 3D insertion site shape. Specimens were then disarticulated, and the boundaries of the ACL insertion sites were digitized using a high-accuracy laser scanner. MRI and laser scan insertion sites were co-registered to determine the percent overlapping area and difference in insertion centroid location.

**Results**—Femoral ACL insertion site area averaged  $112.7 \pm 17.9$  mm<sup>2</sup> from MRI and  $109.7 \pm 10.9$  mm<sup>2</sup> from laser scan ( $p=0.345$ ). Tibial insertion area was  $134.7 \pm 22.9$  mm<sup>2</sup> from MRI and  $135.2 \pm 15.1$  mm<sup>2</sup> from laser scan ( $p=0.881$ ). Percentages of overlapping area between modalities were  $82.2 \pm 10.2$  % for femurs and  $81.0 \pm 9.0$  % for tibias. The root-mean-square differences for ACL insertion site centroids were 1.87 mm for femurs and 2.49 mm for tibias. The MRI-estimated ACL insertion site centroids were biased on average  $0.6 \pm 1.6$  mm proximally and  $0.3 \pm 1.9$  mm posteriorly for femurs, and  $0.3 \pm 1.1$  mm laterally and  $0.5 \pm 1.5$  mm anteriorly for tibias.

**Conclusion**—Errors in ACL insertion site location and area estimated from 3D-MRI were determined via comparison with high-accuracy 3D laser scanning. Results indicate that MRI can provide estimates of ACL insertion site area and centroid location with clinically applicable accuracy. MRI-based assessment can provide a reliable estimate of the native ACL anatomy, which can be helpful for surgical planning as well as assessment of graft tunnel placement.

### Keywords

Knee; Anterior cruciate ligament; Magnetic resonance image; Insertion site

---

Corresponding author: Scott Tashman, Ph.D., Department of Orthopedic Surgery, University of Pittsburgh, 3820 S Water St. Pittsburgh PA 15206 USA., Phone: +1-412-586-3950, FAX: +1-412-586-3979, tashman@pitt.edu.

### Conflict of interest

This study was funded by a Pittsburgh Foundation Grant (M2012-0022).

## Introduction

The goal of anterior cruciate ligament (ACL) reconstruction is to restore normal knee kinematics and to allow patients to return to the previous level of activity and function. Non-anatomic tunnel placement has been previously shown to decrease knee motion and to produce abnormal rotational knee kinematics during dynamic loading [7,22], and may contribute to early progression of osteoarthritis or place grafts at higher risk for failure. Because of these observations, surgical techniques have focused more recently on “anatomic” reconstruction, targeting placement of bone tunnels within the native ACL insertion sites [2,5,9,10,12,25] with the goal to achieve improved clinical and biomechanical outcomes [2,26]. Anatomic reconstruction requires reliable preoperative or inter-operative assessment of the knee joint for proper placement of the graft tunnels [12]. In cases of chronic ACL deficiency or revision surgery, however, it may be difficult to identify the native insertion sites or relevant bony landmarks via arthroscopic examination. Previous studies have supported the use of morphometric reference data from the contralateral (uninjured) side for evaluation knee anatomy [3], suggesting ACL anatomy from the contralateral knee could be used determining ACL insertion site location. Additionally, from a research perspective, non-invasive assessment of native insertion sites provides a basis for precise postoperative evaluation of graft tunnel locations, and can provide insights into the relationships between anatomy and function of the knee and ACL. Thus, preoperative planning, surgical navigation and postoperative assessment of tunnel placement could all benefit significantly from accurate detection of insertion site centers and shapes.

Magnetic resonance image (MRI) has been used previously to non-invasively investigate the ACL insertion sites in relation to the ACL bundles and surrounding anatomical landmarks [8,14,17–21]. These studies, however, addressed only repeatability and precision of insertion site locations and areas. Absolute accuracy for detecting ACL insertion site locations and areas could not be assessed due to the absence of a “gold standard”, high-accuracy measurement for comparison. The methodologies employed also failed to demonstrate expected advantages from using newer, high-resolution imaging sequences for improving accuracy of insertion site location [19].

Therefore, the purpose of this study was to quantify the error in native, uninjured ACL insertion site location and area determination from 3D isotropic MRI in comparison to data obtained via 3D laser scanning of known accuracy. It is hypothesized that there would be no significant differences in ACL insertion site area and centroid location determined from 3D laser scanning and 3D isotropic MRI.

## Materials and Methods

Twelve fresh-frozen ACL-intact cadaver knees (6 paired specimens) were used in this study (2 females and 4 males, age at death  $62.0 \pm 6.7$  years). Knee specimens were screened using fluoroscopy and MRI, and excluded if ligament injury, chondromalacia, prior knee surgery, osteoarthritis or osteophytes or damage to the articular cartilage were found. All specimens were stored at  $-20^{\circ}\text{C}$  and allowed to thaw overnight at room temperature prior to imaging,

dissection and testing. The specimens were kept moistened with physiologic saline solution to prevent dehydration throughout testing.

To enable co-registration of MRI and laser scan data, fiducial markers were rigidly fixed to the specimens prior to imaging. Three small skin incisions were made in thigh and calf, respectively. Three custom fiducial marker spheres were filled with Radiance<sup>®</sup> multimodality fluid (Beekley, Bristol, CT, USA), attached to the heads of polyether-ether-ketone (PEEK) screws, and rigidly bicortically fixated into each femoral and tibial bone shaft (Figure 1). The radiance fluid is clearly visible in MRI, and the external surface of the markers is easily laser scanned and contact probed. Thus, alignment of the centers of the spherical markers between MRI and laser scans can be achieved accurately.

All specimens underwent imaging on a 3T Magnetic Resonance (MR) scanner (MAGNETOM Trio, Siemens, Erlangen, Germany), using a lower extremity knee coil. Images were collected using an isotropic 3D Dual Echo Steady State (DESS) WS sequences (pixel size: 0.45×0.45×0.45 mm, TR: 16 ms, duration 11 minutes). The specimens were fully extended during scanning.

Identification of the femoral and tibial ACL insertion sites were performed using Mimics image processing software (Materialise, Leuven, Belgium). The femoral and tibial bones were manually segmented from the MRIs for all specimens and rendered into 3D surface models. Since the multimodality fluid appears in MRI images with high contrast, the fiducial co-registration spheres were easily segmented from surrounding tissues using a simple pixel thresholding function. The ACL insertion sites were manually identified on axial and coronal planes for femurs and sagittal and coronal planes for tibias (Figure 2). For the identification process, the ligament-bone interface was manually marked by iteratively placing points on the insertion site boundary in each slice and adjusting placements by manually comparing to neighboring image slices. This process was repeated by the operator at least three times for each insertion site identification, with care taken not to misidentify near the extreme edges of the ligament insertions (which could be affected by volume averaging of the MRI). While visualizing the 3D bone surface model in conjunction with the slice-by-slice insertion site outlines, the inner insertion region points were deleted, leaving only the outer boundary points of the ACL footprint.

After imaging, femurs and tibias were disarticulated and the ACL insertion sites were observed macroscopically. All specimens were dissected and the boundaries of the ACL insertion sites were marked with ink. A 3D laser scanner and contact probe (FaroArm<sup>®</sup> Platinum, FARO Technologies Inc., Lake Mary, FL, USA) was used to obtain a 3D surface profile of the knee, marked insertion boundaries, and co-registration spheres (Figure 3). This coordinate measurement system employs laser projection and sensors to enable detailed non-contact 3D measurement of surface geometry for nearly any shape object. The volumetric accuracy and single point repeatability of the FaroArm are 0.036 mm and 0.043 mm, respectively [15,24]. With errors in the order of ten times smaller than the MRI voxel size, measurements from this system provide a suitable “gold standard” reference for assessing MRI measurement accuracy. Femoral and tibial bone shafts were rigidly clamped into place to facilitate scanning using the FaroArm ACL insertion boundaries and the co-registration

spheres were digitized. Laser scans of the bone and cartilage surfaces were also acquired to provide reference frames for the probe data. Laser scan point clouds of the femurs, tibias, and co-registration spheres were rendered as mesh models within Geomagic software (Geomagic, Durham, NC, USA).

Co-registration between MRI and laser scan modalities was performed in Geomagic using the fiducial spheres (Figure 4). Spheres were fit separately to the MRI-derived and FaroArm-derived models of the fiducial co-registration spheres in Geomagic. Matching pairs of the three spheres fixed to each bone were aligned together in a least-squares sense to obtain the transformation from MRI coordinate system to the FaroArm for each femur and tibia. By applying the resulting transformation to the MRI-derived 3D insertion boundary points, the MRI-based and FaroArm-based insertion site boundaries could be expressed in a common global coordinate system and visually overlaid (Figure 4).

Anatomical coordinate systems were determined for femurs and tibias using the methods proposed by Miranda et al. and Scanlan et al.[11,14], in order to express the errors and biases in a clinically meaningful reference frame. For femurs, the medial-lateral (M-L) axis was defined by fitting a cylinder to the posterior aspect of the femoral condyles of the MRI-derived surface model. The axis of the cylinder extended from the most medial to the most lateral aspect of the posterior femoral condyles and the femoral coordinate system origin was located at the midpoint of this axis. The center of a circle fit to the most proximal cross-section of the femoral shaft was used to create a temporary proximal-distal (P-D) axis, and the line perpendicular to these two axes was defined as the anterior-posterior (A-P) axis. The final P-D axis was chosen in the direction perpendicular to the M-L and A-P axes. For tibias, a plane of best-fit was calculated for the isolated proximal tibial plateau in Geomagic. The tibial M-L axis was defined as the vector connecting the most medial and lateral points of tibial plateau on this plane. The P-D axis was set as the normal vector of this plane. Then, the A-P axis was defined as the vector perpendicular to these two axes. The ACL insertion site boundaries estimated from MRI and acquired from the FaroArm were exported into custom MATLAB (MATLAB, The Math Works, Natick, MA, USA) software that projected insertion boundaries into the sagittal anatomical plane for the femur and into the transverse plane for the tibia. The software generated 2D meshes of the closed ACL attachment boundaries and calculated the area and geometric centroid of the insertion. The percentage overlapping area and the difference in centroid location estimated from MRI and the FaroArm were assessed. Errors in centroid estimation were resolved into components along the anatomical axes. These experiment protocols were performed after approval of Office for Oversight of Anatomic Specimens in University of Pittsburgh (#461).

### Statistical analysis

To determine the intra- and inter-observer reliabilities of the MRI estimation of insertion site area and centroid location, three investigators (blinded to the specimen identifications) performed MRI measurements twice on four randomly selected knee specimens. The intra- and inter-observer reliabilities of all radiographic measurements were evaluated using intra-class correlation coefficients (ICCs). The ICCs for intra- and inter-observer reliability were  $> 0.85$  (range, 0.86 – 0.95) for all measurements. Based on this observed reliability,

measurements taken by a single investigator were used for the remaining analyses. Differences in insertion site area between the MRI and laser scan measurements were assessed with paired t-tests. Root mean square (RMS) errors were calculated for centroid locations. Statistical calculation were performed in StatView (StatView; SAS Institute, Cary, NC, USA) with significance level set at  $P < 0.05$ . A power analysis was performed with G\* power 3.1.9.2 (Heinrich-Heine-Universität, Düsseldorf, Germany) with a sample size of 12 specimens, power was 0.71 for an effect size of 0.8 and an  $\alpha$  error of 0.05.

## Results

### MRI and laser scan co-registration accuracy

Average co-registration error of the fiducial spheres trios between MRI and laser scanning was  $0.6 \pm 0.5$  mm for femurs and  $0.7 \pm 0.2$  mm for tibias (mean  $\pm$  standard deviation).

### ACL insertion site area

Estimates of ACL insertion site areas were similar between MRI and laser scans (Figure 5). Femoral insertion site area averaged  $112.7 \pm 17.9$  mm<sup>2</sup> from MRI and  $109.7 \pm 10.9$  mm<sup>2</sup> from laser scans (*n.s.*). Tibial insertion site area was  $134.7 \pm 22.9$  mm<sup>2</sup> from MRI and  $135.2 \pm 15.1$  mm<sup>2</sup> from laser scans (*n.s.*). Percentage overlapped area of ACL insertion sites were  $82.2 \pm 10.2$  % for femurs and  $81.0 \pm 9.0$  % for tibias.

### ACL insertion site centroid location

RMS errors in MRI-estimated ACL insertion site centroids (relative to laser scan data) were 1.87 mm for femurs and 2.49 mm for tibias (Table 1). Relative to the reference centroid locations (determined from laser scanning), the MRI-estimated insertion sites were located on average  $0.6 \pm 1.6$  mm proximally and  $0.3 \pm 1.9$  mm posteriorly for femurs, and  $0.3 \pm 1.1$  mm laterally and  $0.5 \pm 1.5$  mm anteriorly for tibias.

## Discussion

The most important finding of the present study was that MRI-based estimates of ACL insertion site geometry, using the sequence and methodology described, are consistently close to reference laser scan measurement. Insertion site areas overlapped by an average of 80 % between the two measurements. Differences in the centroid locations of ACL insertion sites were small for both femoral and tibial ACL insertion sites, averaging approximately 2 mm.

Accurate detection of ACL insertion sites from MRI is a challenging problem. While previous studies have described the identification of ACL insertion sites from MRI [1,6,8,14,18–20], none have comprehensively assessed the absolute accuracy of both insertion site area and location. Swami et al. reported that variability across observers for estimating the 3D center of ACL attachments from clinical MRI was similar to the MRI slice thickness [18], and reported similar inter-observer reliability with 2D or 3D sequences [19]. But, these studies assessed only repeatability, not absolute accuracy. Abebe et al. did assess absolute accuracy for location ACL attachments from MRI [1]. This single-specimen study,

however could not account for the previously reported natural variation in ACL attachment shape and location [3]. The current study utilized multiple specimens to validate the accuracy of determining ACL insertion centers from an isotropic 3D MRI sequence, employing a true “gold standard” high-accuracy measurement (dissection and co-registered laser scanning) for comparison. The resulting accuracy is similar to the level of precision that could be expected for surgical tunnel placement (in the hands of an experienced surgeon), suggesting that 3D MR imaging has the potential to allow surgeons to preoperatively template tunnel position according to a patient’s individual anatomy.

While small biases (0.3 – 0.6 mm) were identified between the MRI and laser scan measurements, these discrepancies may be due to the morphology of ACL as it connects to the insertion sites. ACL insertions consist of central fibers that connect linearly, along with so-called “indirect” fibers that fan out at the insertion site [13,16,23]. Even with a high-resolution MRI sequence (0.45 mm voxels sizing) there is a limit in the ability to detect the very small or thin features of the fan-like region of the ACL due to partial volume averaging. Therefore, misidentification of this “indirect” region may create an apparent shift in the estimated centroid location of femoral ACL insertion sites from MRI. For tibias, misidentification of the meniscal root might also introduce errors in MRI measurements. Despite these discrepancies, original ACL insertion site geometry was estimated within 80 % using the isotropic MRI sequences.

Several limitations are noted for this study. First, a relatively small sample size and the use of primarily older specimens may have affected the results. The 12 knees assessed in this study cannot provide a comprehensive assessment of the effects of ACL shape and location variability. It is also unknown if the appearance of ACL insertion sites on MRI varies with age. Some error was inevitably introduced during the process of co-registering the MRI and laser scan datasets, though the co-registration errors were typically small. Thirdly, the ligaments imaged in this experiment were from cadaveric specimens with intact ACL’s, which might not be representative of living human ligaments, nor any of the typical pathologies seen in ACL reconstruction patients including hemorrhage, edema, and ligament attenuation or discontinuity. Finally, the size of the cadaver knees or the body mass index of cadaver specimens were not controlled. Therefore, the extent of the soft tissue envelope around the ACL may affect the results.

Despite these limitations, these results suggest that anatomical ACL insertion sites can be reliably and accurately identified using isotropic 3D MRI sequences. MRI-based assessment of ACL insertion site anatomy has many research applications, including assessing the natural variability in knee geometry, evaluating the relationships between insertion site location/shape and knee function and determining how well graft tunnel locations overlay with native insertion sites (obtained from the MRI of contralateral, uninjured) knees). Comparing ACL anatomy of injured and matched uninjured populations may also provide insight into the possible role of ACL anatomy as a risk factor for injury.

The primary clinical application for the method described here is preoperative planning prior to ACL reconstruction. No attempt was made to directly assess insertion site geometry from ACL-injured knees, which may be problematic given the tissue disruption and rapid

deterioration of the ACL stump after rupture [4]. However, while there may be significant variability in the shape and location of ACL insertion sites between individuals, side-to-side symmetry between limbs within individuals is high [3]. Thus utilizing the methodology reported here, MRI of the contralateral leg could provide a reasonable estimate of the native ACL anatomy for the injured knee. While contralateral knee imaging may not be practical for routine clinical procedures, the method employed for this study could be particularly beneficial for revision procedures or treating chronic injuries (where the native ACL anatomy is no longer visible arthroscopically and bony landmarks may have been disrupted by prior surgery), and could provide precise anatomical reference for image-guided surgical systems.

Future work will apply these methodologies to validate the more clinically prevalent 3 mm planar MRI sequences in determining insertion centers, assessing the natural variation in centroid location and shape in an *in-vivo* database of isotropic 3D MRI knee scans, and the optimization of MRI scan parameters to provide the best imaging of the ACL attachment.

## Conclusion

The error in ACL insertion site location and area estimated from 3D isotropic MRI was quantified using high-accuracy 3D laser scanning and contact probing as a gold standard in ACL-intact knees. Results that 3D isotropic MRI scans can provide clinically useful estimates of ACL insertion site area and centroid location, with high accuracy and repeatability. MRI-based assessment can provide a reliable estimate of the native ACL anatomy, which can be helpful for surgical planning as well as assessment of graft tunnel placement.

## References

1. Abebe ES, Moorman CT 3rd, Dziedzic TS, Spritzer CE, Cothran RL, Taylor DC, Garrett WE Jr, DeFrate LE. Femoral tunnel placement during anterior cruciate ligament reconstruction: an in vivo imaging analysis comparing transtibial and 2-incision tibial tunnel-independent techniques. *Am J Sports Med.* 2009; 37(10):1904–1911. [PubMed: 19687514]
2. Abebe ES, Utturkar GM, Taylor DC, Spritzer CE, Kim JP, Moorman CT 3rd, Garrett WE, DeFrate LE. The effects of femoral graft placement on in vivo knee kinematics after anterior cruciate ligament reconstruction. *J Biomech.* 2011; 44(5):924–929. [PubMed: 21227425]
3. Dargel J, Feiser J, Gotter M, Pennig D, Koebke J. Side differences in the anatomy of human knee joints. *Knee Surg Sports Traumatol Arthrosc.* 2009; 17(11):1368–1376. [PubMed: 19633830]
4. Edwards A, Bull AM, Amis AA. The attachments of the anteromedial and posterolateral fibre bundles of the anterior cruciate ligament. Part 2: femoral attachment. *Knee Surg Sports Traumatol Arthrosc.* 2008; 16(1):29–36. [PubMed: 17957351]
5. Fu FH, Musahl V. Anatomic ACL reconstruction. Preface. *Clin Sports Med.* 2013; 32(1):xv–xvi.
6. Han Y, Kurzencwyg D, Hart A, Powell T, Martineau PA. Measuring the anterior cruciate ligament's footprints by three-dimensional magnetic resonance imaging. *Knee Surg Sports Traumatol Arthrosc.* 2012; 20(5):986–995. [PubMed: 21987362]
7. Harner CD, Irrgang JJ, Paul J, Dearwater S, Fu FH. Loss of motion after anterior cruciate ligament reconstruction. *Am J Sports Med.* 1992; 20(5):499–506. [PubMed: 1443315]
8. Ichiba A, Kido H, Tokuyama F, Makuya K, Oda K. Sagittal view of the tibial attachment of the anterior cruciate ligament on magnetic resonance imaging and the relationship between anterior cruciate ligament size and the physical characteristics of patients. *J Orthop Sci.* 2014; 19(1):97–103. [PubMed: 24141392]

9. Kato Y, Maeyama A, Lertwanich P, Wang JH, Ingham SJ, Kramer S, Martins CQ, Smolinski P, Fu FH. Biomechanical comparison of different graft positions for single-bundle anterior cruciate ligament reconstruction. *Knee Surg Sports Traumatol Arthrosc.* 2013; 21(4):816–823. [PubMed: 22419266]
10. Mae T, Shino K, Matsumoto N, Hamada M, Yoneda M, Nakata K. Anatomical two-bundle versus Rosenberg's isometric bi-socket ACL reconstruction: a biomechanical comparison in laxity match pretension. *Knee Surg Sports Traumatol Arthrosc.* 2007; 15(4):328–334. [PubMed: 17096174]
11. Miranda DL, Rainbow MJ, Leventhal EL, Crisco JJ, Fleming BC. Automatic determination of anatomical coordinate systems for three-dimensional bone models of the isolated human knee. *J Biomech.* 2010; 43(8):1623–1626. [PubMed: 20167324]
12. Murawski CD, van Eck CF, Irrgang JJ, Tashman S, Fu FH. Operative treatment of primary anterior cruciate ligament rupture in adults. *J Bone Joint Surg Am.* 2014; 96(8):685–694. [PubMed: 24740666]
13. Sasaki N, Ishibashi Y, Tsuda E, Yamamoto Y, Maeda S, Mizukami H, Toh S, Yagihashi S, Tonosaki Y. The femoral insertion of the anterior cruciate ligament: discrepancy between macroscopic and histological observations. *Arthroscopy.* 2012; 28(8):1135–1146. [PubMed: 22440794]
14. Scanlan SF, Lai J, Donahue JP, Andriacchi TP. Variations in the three-dimensional location and orientation of the ACL in healthy subjects relative to patients after transtibial ACL reconstruction. *J Orthop Res.* 2012; 30(6):910–918. [PubMed: 22105556]
15. Shahmiri R, Aarts JM, Bennani V, Atieh MA, Swain MV. Finite element analysis of an implant-assisted removable partial denture. *J Prosthodont.* 2013; 22(7):550–555. [PubMed: 23551664]
16. Smigielski R, Zdanowicz U, Drwiega M, Ciszek B, Ciszewska-Lyson B, Siebold R. Ribbon like appearance of the midsubstance fibres of the anterior cruciate ligament close to its femoral insertion site: a cadaveric study including 111 knees. *Knee Surg Sports Traumatol Arthrosc.* 2015; 23(11):3143–3150. [PubMed: 24972997]
17. Staeubli HU, Adam O, Becker W, Burgkart R. Anterior cruciate ligament and intercondylar notch in the coronal oblique plane: anatomy complemented by magnetic resonance imaging in cruciate ligament-intact knees. *Arthroscopy.* 1999; 15(4):349–359. [PubMed: 10355709]
18. Swami VG, Cheng-Baron J, Hui C, Thompson R, Jaremko JL. Reliability of estimates of ACL attachment locations in 3-dimensional knee reconstruction based on routine clinical MRI in pediatric patients. *Am J Sports Med.* 2013; 41(6):1319–1329. [PubMed: 23576685]
19. Swami VG, Cheng-Baron J, Hui C, Thompson RB, Jaremko JL. Reliability of 3D localisation of ACL attachments on MRI: comparison using multi-planar 2D versus high-resolution 3D base sequences. *Knee Surg Sports Traumatol Arthrosc.* 2015; 23(4):1206–1214. [PubMed: 24651978]
20. Swami VG, Mabee M, Hui C, Jaremko JL. MRI Anatomy of the Tibial ACL Attachment and Proximal Epiphysis in a Large Population of Skeletally Immature Knees: Reference Parameters for Planning Anatomic Physal-Sparing ACL Reconstruction. *Am J Sports Med.* 2014; 42(7):1644–1651. [PubMed: 24755252]
21. Tanaka Y, Shiozaki Y, Yonetani Y, Kanamoto T, Tsujii A, Horibe S. MRI analysis of the attachment of the anteromedial and posterolateral bundles of anterior cruciate ligament using coronal oblique images. *Knee Surg Sports Traumatol Arthrosc.* 2011; 19(Suppl 1):S54–59. [PubMed: 21533538]
22. Tashman S, Collon D, Anderson K, Kolowich P, Anderst W. Abnormal rotational knee motion during running after anterior cruciate ligament reconstruction. *Am J Sports Med.* 2004; 32(4):975–983. [PubMed: 15150046]
23. Tsukada S, Fujishiro H, Watanabe K, Nimura A, Mochizuki T, Mahakkanukrauh P, Yasuda K, Akita K. Anatomic variations of the lateral intercondylar ridge: relationship to the anterior margin of the anterior cruciate ligament. *Am J Sports Med.* 2014; 42(5):1110–1117. [PubMed: 24603528]
24. Viste A, Trouillet F, Testa R, Cheze L, Desmarchelier R, Fessy MH. An evaluation of CT-scan to locate the femoral head centre and its implication for hip surgeons. *Surg Radiol Anat.* 2014; 36(3):259–263. [PubMed: 23881154]
25. Yasuda K, Tanabe Y, Kondo E, Kitamura N, Tohyama H. Anatomic double-bundle anterior cruciate ligament reconstruction. *Arthroscopy.* 2010; 26(9 Suppl):S21–34. [PubMed: 20810091]



26. Yasuda K, van Eck CF, Hoshino Y, Fu FH, Tashman S. Anatomic single- and double-bundle anterior cruciate ligament reconstruction, part 1: Basic science. *Am J Sports Med.* 2011; 39(8): 1789–1799. [PubMed: 21596902]

Author Manuscript

Author Manuscript

Author Manuscript

Author Manuscript

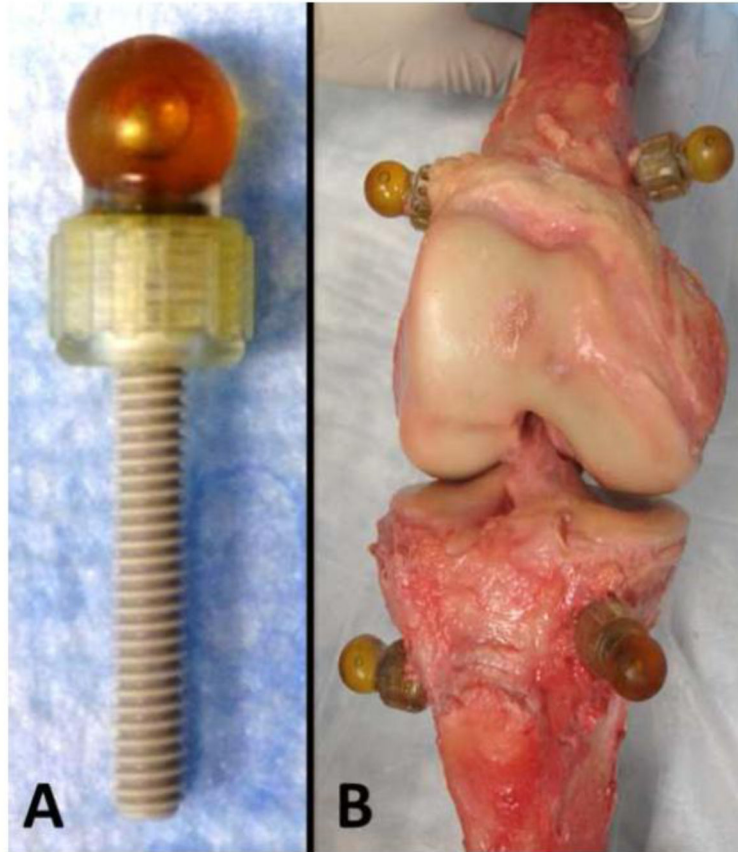


**Figure 1.**

A) Fiducial marker spheres filled with Radiance<sup>®</sup> multimodality fluid with polyether-etherketone (PEEK) screw.

B) The screws with markers were attached to femur and tibia. Specimens were disarticulated before obtaining the gold standard data using the laser scan.

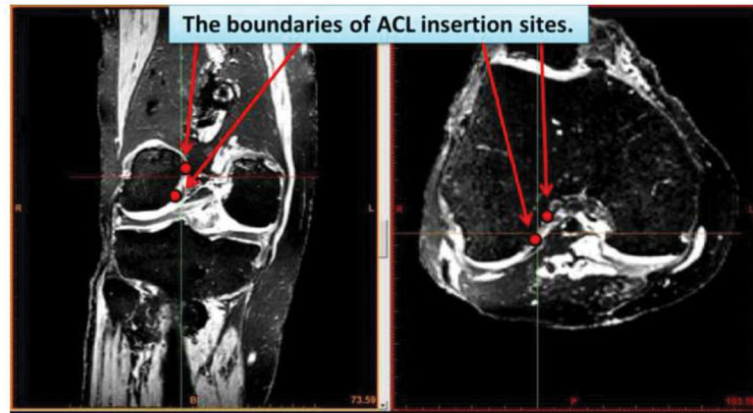


**Figure 2.** The ACL insertion sites were identified on axial and coronal planes for femur and sagittal and coronal planes for tibia. After the identification process, the ACL insertion site boundaries were converted to the 3D data and displayed on the 3D bone surfaces.

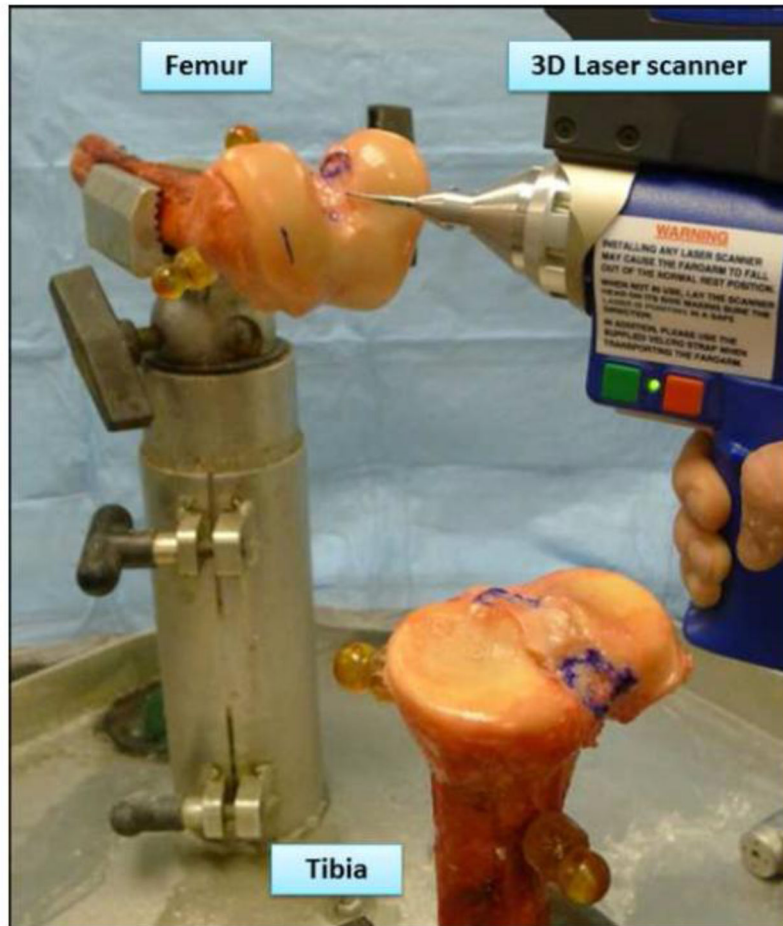


**Figure 3.** The 3D profile of the knee was obtained by use of a 3D laser scanner (FaroArm<sup>®</sup> Platinum, FARO Technologies Inc., Lake Mary, FL, USA).

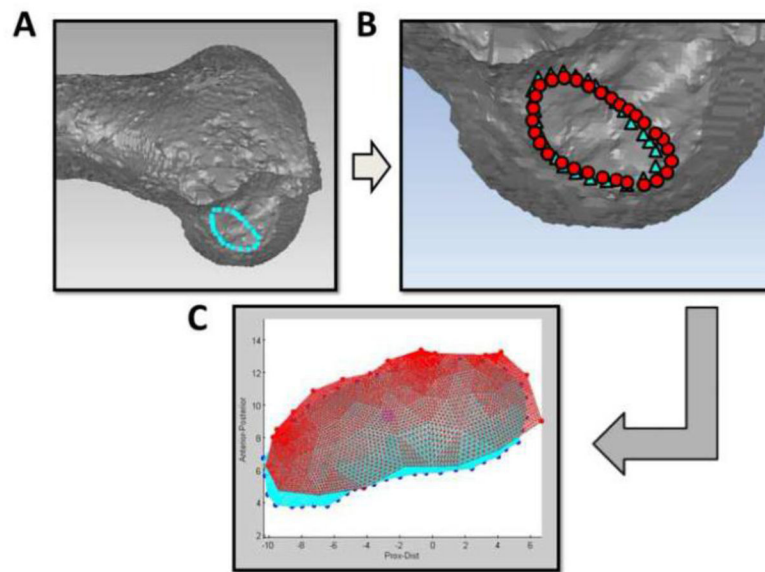


**Figure 4.**

- A) The boundaries of ACL insertion sites determined from MRI were imported into Geomagic software (Geomagic, Durham, NC, USA).
- B) Co-registration between MRI and laser scan data was performed in Geomagic software (○: MRI data, △: Laser scan data).
- C) The ACL insertion sites area and centroid locations from MRI and laser scan were compared in custom MATLAB software (MATLAB, The Math Works, Natick, MA, USA).

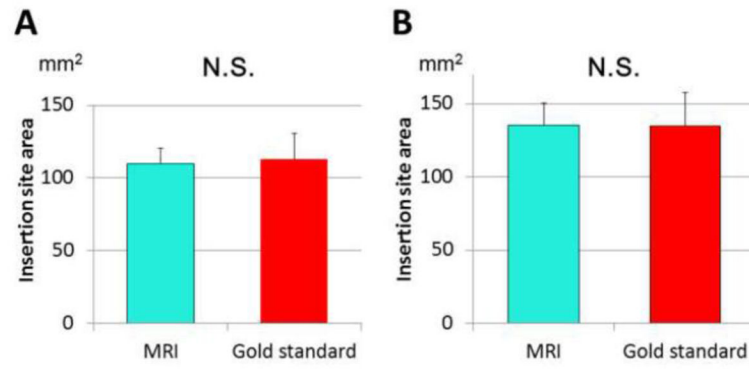


**Figure 5.**  
A) Femoral ACL insertion site area (mm<sup>2</sup>)  
B) Tibial ACL insertion site area (mm<sup>2</sup>)

**Table 1**

## Comparison of the insertion sites

	<b>Femur</b>	<b>Tibia</b>
Percentage overlapping area (%)	82.2 ± 10.2	81.0 ± 9.0
Centroid RMS error (mm)	1.87	2.49
Centroid bias		
A/P direction (mm)	-0.3 ± 1.1	0.5 ± 1.5
P/D direction (mm)	0.6 ± 1.6	
M/L direction (mm)		-0.3 ± 1.9

(Mean ± Standard deviation)

Abbreviations: A/P: Anterior/Posterior (Anterior as positive value)

P/D: Proximal/Distal (Proximal as positive value)

M/L: Medial/Lateral (Medial as positive value)

RMS: Root mean square